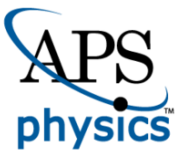

Compatibility of causal hidden-variable theories with a delayed-choice experiment

He-Liang Huang, Yi-Han Luo, B. Bai, Y.-H. Deng, H. Wang, Q. Zhao, H.-S. Zhong, Y.-Q. Nie, W.-H. Jiang, X.-L. Wang, Jun Zhang, Li Li, Nai-Le Liu, Tim Byrnes, J. P. Dowling, Chao-Yang Lu, and Jian-Wei Pan

Phys. Rev. A **100**, 012114 — Published 15 July 2019

DOI: 10.1103/PhysRevA.100.012114

On the compatibility of causal hidden-variable theories with the delayed-choice experiment

He-Liang Huang,[1,2,3] Yi-Han Luo,[1,2] B. Bai,[1,2] Y.-H. Deng,[1,2] H. Wang,[1,2] Q. Zhao,[4]
H.-S. Zhong,[1,2] Y.-Q. Nie,[1,2] W.-H. Jiang,[1,2] X.-L. Wang,[1,2] Jun Zhang,[1,2] Li Li,[1,2]
Nai-Le Liu,[1,2] Tim Byrnes,[5,6,7] J. P. Dowling,[8,1,6] Chao-Yang Lu,[1,2] and Jian-Wei Pan[1,2]

[1]*Hefei National Laboratory for Physical Sciences at Microscale and Department of Modern Physics, University of Science and Technology of China, Hefei, Anhui 230026, China*
[2]*CAS Centre for Excellence and Synergetic Innovation Centre in Quantum Information and Quantum Physics, University of Science and Technology of China, Hefei, Anhui 230026, China*
[3]*Henan Key Laboratory of Quantum Information and Cryptography, Zhengzhou, Henan 450000, China*
[4]*Center for Quantum Information, Institute for Interdisciplinary Information Sciences, Tsinghua University, Beijing 100084, China*
[5]*New York University Shanghai, 1555 Century Ave, Pudong, Shanghai 200122, China*
[6]*NYU-ECNU Institute of Physics at NYU Shanghai, 3663 Zhongshan Road North, Shanghai 200062, China*
[7]*Department of Physics, New York University, New York, NY 10003, USA*
[8]*Hearne Institute for Theoretical Physics, Department of Physics and Astronomy, Louisiana State University, Baton Rouge, Louisiana 70803, USA*

(Dated: June 4, 2019)

Wheeler's delayed-choice experiment investigates the indeterminacy of wave-particle duality and the role played by the measurement apparatus in quantum theory. Due to the inconsistency with classical physics, it has been generally believed that it is not possible to reproduce the delayed-choice experiment using a hidden variable theory. Recently, it was shown that Wheeler's delayed-choice experiment can be explained by a causal two dimensional hidden-variable theory [R. Chaves, G. B. Lemos, and J. Pienaar, Phys. Rev. Lett. 120, 190401 (2018)]. Here, we carry out a delayed-choice experiment by using photon states that are space-like separated, and demonstrate that the experiment is consistent with quantum theory but inconsistent with any causal two-dimensional hidden variable theory in a device-independent manner. This demonstrates that causality can be used to test quantum theory in a complementary way to the Bell and Leggett-Garg tests.

After the two famous Bohr-Einstein debates of 1927 and 1930 on the validity of the quantum theory [1], Einstein had to accept that quantum mechanics was correct. However, in his paper with Podolsky and Rosen (EPR) [2], EPR claimed that quantum theory, while not incorrect, was incomplete. That paper showed that quantum-entangled states had elements of nonlocality, un-reality, and uncertainty that no "sensible" theory should have. The EPR paper opened the door for a replacement theory for quantum mechanics, now called a hidden variable (HV) theory, that would be more like a classical statistical theory, where the statistics were governed by HVs that were either unknown or unaccessable. Von Neumann then provided a proof that no HV theory could reproduce all the predictions of quantum theory [3]. Later, Bohm produced a HV theory that reproduced all the predictions of nonrelativistic quantum theory. To solve this apparent paradox, Bell showed that von Neumann had made an explicit assumption that the HV theory was local, but that the HV theory of Bohm was nonlocal — that is actions at one place could affect outcomes far away in apparent violation of Einstein causality [4]. Thus, it is important to make the locality requirement explicit and show whether local HV theory could reproduce the predictions of quantum theory.

In an effort to challenge quantum mechanics, and make quantum predictions consistent with common sense, it was suggested that quantum particles can actually "know" in advance to which experiment they are going to be confronted through a HV, and thus can determine which behavior to show. For example, the photon could "decide" whether it was going to behave as a particle or behave as a wave before it reach the detection device in the double-slit experiment. However, Wheeler published two theory papers, now called Wheeler's delayed-choice experiments (WDCE), that claimed to exclude the causal link between the experimental setup and a HV that predefines the photons behavior, and point out that complementarity and wave-particle duality alone contained an element of Einstein nonlocality [5, 6]. Fig. 1(a) shows an example of an implementation of WDCE, where a photon enters an Mach-Zehnder interferometer (MZI). The observer randomly chooses whether or not to insert the second beamsplitter (BS_2) after the photon has passed through BS_1, thereby observing interference (wave-like behavior) or no interference (particle-like behavior) accordingly. By delaying the choice of the configuration until well after the photon passes BS_1, this ensures that it could not "know" which behavior it should show in advance. So far, WDCE has been implemented experimentally in various quantum systems [7–12]. Interestingly, a recent extension, quantum delayed-choice experiment (QDCE), suggested using a quantum beam splitter at the interferometer's output [13, 14], enabling one to project the testing photon into an arbitrary coherent wave-particle superposition, and motivated many QDCE experiments [15–18]. In short, until recently experimental demonstrations of WDCE (or QDCE) were thought to have perfectly ruled out the possible of quantum behavior induced by HV.

Chaves, Lemos, and Pienaar recently revisited WDCE, and showed using methods in causal inference [19, 20] that the original WDCE and QDCE can in fact be modeled by a causal two dimensional HV theory [21]. The HV theory they suggest follows the same causal structure of the experiment shown in Fig. 1(a), such that statistics produced by the final detection can be determined from a HV and the information of the type

of measurement being performed. To overcome this shortcoming, the authors suggested a modified version of WDCE (MWDCE, Fig. 1(b)) that cannot be explained by a causally structured HV theory, assuming a HV dimension of two. In the modified setup, the second beamsplitter is always put in place, and the two types of detection is controlled by the phase shifter β_j. The additional component is that Alice has the ability to prepare a set of states, controlled by her own phase shifter α_i. Here, an important aspect is that Alice and Bob's devices are independent. In Ref. [21] it is shown that this new setup can no longer be modeled by a causally structured HV theory, as long as the HV has a dimension of two. Such a causal HV theory can be distinguished from a genuine quantum theory by comparing the statistics to a device-independent prepare and measure (PAM) scenario [22, 23] (Fig. 1(c)). Using the statistics of the measurements and the setting values, a device-independent dimension witness [22] can be constructed that is capable of distinguishing between a causally structured HV theory. The dimensional witness can, in principle, work with any transmittance strictly larger than zero, thus making MWDCE can be demonstrated in the presence of arbitrarily low detection efficiency.

In this paper, we carry out a demonstration of the MWDCE in a device-independent manner. By measuring a device-independent witness we verify that two-dimensional causally structured HV theory can indeed be ruled out. We furthermore rule out the prior correlations that may exist between Alice and Bob by violation of a dimension witness inequality. Finally, we quantify the degree of retrocausality that would be required to reproduce our experiments, placing bounds on such hypothetical scenarios. We note that in the MWDCE of Fig. 1(b), and also in our experiment, the second beamsplitter is always in place. Thus the focus of our experiment is whether the WDCE in this setting can be explained by using a causally structured classical HV theory, rather than testing wave-particle duality. It is therefore complementary to tests of nonlocality in quantum theory such as in a Bell test or a Leggett-Garg test [24].

Figure 1(d) shows the schematic experimental implementation for realizing the MWDCE. The path-based interferometer as shown in Fig. 1(b) is implemented in our experiment by a polarization-based interferometer, which has the advantage of superior stability. The horizontal (H) and vertical (V) polarizations correspond to the upper and lower paths in the MZI in Fig. 1(b). To prepare the various initial states we use an EPR photon pair emitter located at Charlie's location C. Charlie is located closer to Alice than to Bob to allow Alice to make her preparation step first by measuring her half of the entangled pair after applying her polarization rotation α_i first. This collapses Bob's half of the entangled pair into a single photon to which Alice's polarization rotation α_i has been applied. Then Bob applies his polarization rotation β_j, before any influence from Alice can reach him, and measures the photon through a polarizing beam splitter (PBS) and detectors. We note that the use of the Bell state is merely to prepare a random state for Bob, and the entanglement plays no further role. In the experiment, we synchronize the clock and control the delay of every device carefully to ensure the time order of preparation and

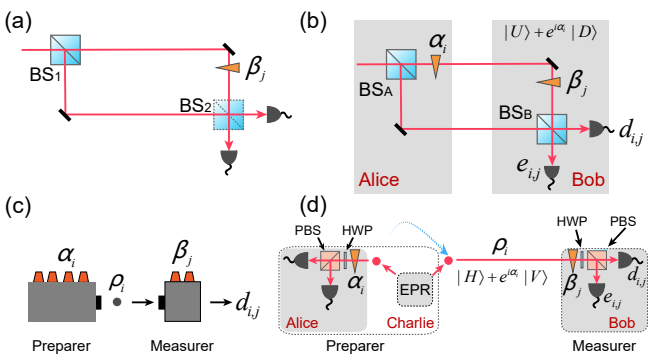

FIG. 1. Various configurations of the delayed-choice experiment. (a) Wheeler's delayed-choice experiment (WDCE). (b) The modified WDCE (MWDCE). The gray areas correspond to Alice (preparer) and Bob (measurer), respectively. In the modified setup, the second beamsplitter is always put in place, Alice has the ability to prepare a set of states, controlled by her own phase shifter $\alpha_i \in \{\alpha_0 = 0, \alpha_1 = \pi, \alpha_2 = -\pi/2, \alpha_3 = \pi/2\}$, and two types of detection is controlled by the phase shifter $\beta_j \in \{\beta_0 = \pi/2, \beta_1 = 0\}$ of Bob. The U is the upper path and D is the lower path. (c) The device-independent prepare-and-measure (PAM) scenario for the MWDCE. An initial black-box prepares different physical systems (upon pressing a button labeled by α_i) that are then sent to a second black-box where the systems are measured (upon pressing a button labeled by β_j) to produce an outcome labeled by d_{ij}. (d) Schematic experimental description performed in this paper. Alice prepares a photon by measuring an Bell state in one of two basis, producing four possible states $|H\rangle + e^{i\alpha_i}|V\rangle$. Bob then applies a phase shift and interferes the photon using a PBS to obtain the output.

measurement operation, such that it meets the requirements of the PAM scenario and delayed-choice experiment. Time ordering is now important in the current scheme.

Our experimental setup is shown in Fig. 2. At Charlie's location, an ultraviolet laser pulse with a central wavelength of 394 nm passes through a β-barium borate (BBO) crystal to produce a polarization-entangled pairs $|\Psi^+\rangle_{AB} = |H\rangle_A|V\rangle_B + |V\rangle_A|H\rangle_B$ (normalization coefficients are omitted for brevity) [25]. A half-wave plate (HWP) is placed on one output of the EPR source to produce the Bell state $|\Phi^+\rangle_{AB} = |H\rangle_A|H\rangle_B + |V\rangle_A|V\rangle_B$. The two photons are then coupled to a single mode fiber and sent to Alice (preparer) and Bob (measurer), respectively. The distance between Alice and Bob is 46 m, and the length of the fiber from the entanglement source (Charlie) to Alice is shorter than that to Bob. The electro-optic modulator (EOM) then applies a phase shift of 0 or $\pi/2$ chosen by a quantum random number generator (QRNG) such that Alice's photon is measured in one of two bases $\{|H\rangle_A \pm |V\rangle_A\}$ or $\{|H\rangle_A \pm i|V\rangle_A\}$. For a given basis choice, this causes Bob's part of the Bell state to randomly collapse to one of two states, giving a total of four outcomes $|H\rangle_B \pm |V\rangle_B$ and $|H\rangle_B \mp i|V\rangle_B$. Bob then deploys his delayed-choice of applying one of two polarization rotations $\beta_j \in \{\beta_0 = \pi/2, \beta_1 = 0\}$, chosen by another QRNG. This is equivalent to measuring his photon in one of the two bases $\{|H\rangle_B \pm e^{i\beta_j}|V\rangle_B\}$ chosen by β_j. Two synchronized signals from a central clock are used to trigger the

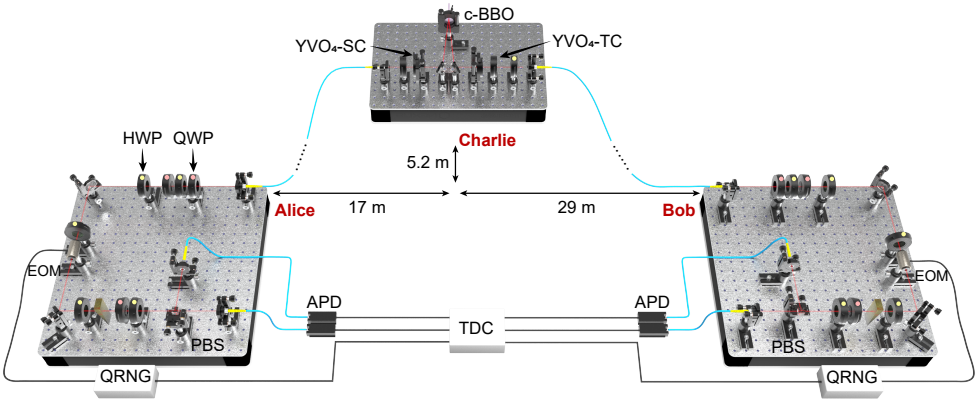

FIG. 2. Experimental setup. The polarization-entangled photon pairs produced by SPDC are coupled into the single-mode fiber and sent to Alice (preparer) and to Bob (measurer), respectively. The distance between Alice and Bob is 46 meters and the length of the fiber from the entanglement source (Charlie) to Alice is shorter than that to Bob (the fiber lengths of Charlie-Alice and Charlie-Bob are 28 meters and 33 meters, respectively). Alice's photon passes through an EOM, then is measured by the APD which collapses Bob's state to $|H\rangle_B + e^{i\alpha_j}|V\rangle_B$ with $\alpha_j \in \{0, \pi, \pm\pi/2\}$, thereby preparing the state. Bob's photon then passes through another EOM where a random phase $\beta_j \in \{\pi/2, 0\}$ is applied to the vertical polarization component, and is finally measured by the APD. The measurement basis of Alice and Bob are each randomly determined by two independent and space-like separated QRNGs and EOMs. In order to meet the delayed-choice condition, the measurement basis of Bob is chosen much later than that of Alice.

two QRNGs to meet the delayed-choice condition. We note that the four preparation states are produced by a combination of Alice's QRNG and the random collapse of the Bell state. Thus no postselection is performed to prepare the state.

In our experiment, the device-independent dimension witness in Ref. [22] is used to exclude the two-dimensional nonretrocausal classical model in MWDCE. However, the premise of using the dimension witness is that the preparer and measurer in the PAM model must be independent. Fortunately, the use of entanglement in our experiment makes this assumption easy to achieve. Specifically, in our experiment, space-like separation is built to ensure that the QRNGs and the photon measurements are both outside their mutual lightcones (Fig. 3(a)). In addition, the QRNGs must fire outside the light cone of the EPR source to ensure that Charlie cannot influence the outcome of the QRNGs, as shown in Fig. 3(b). Thus, the use of entanglement and space-like separations in our experiment rules out potential communication between the preparer and measurer. The assumption of independent devices is required to use the dimension witness of Ref. [22]. By having a space-like separation we can guarantee that no communication can occur between the devices. However, a space-like separation may still possess predetermined classical correlations which make the two devices dependent. In order to deal with potential classical correlations, the dimension witness of Refs. [23, 26] is applied.

To test the two dimensional witness [22], we measure the conditional probability that detector d fires for given settings (α_i, β_j) chosen by Alice and Bob respectively. The matrix elements of the 2×2 dimensional witness matrix W is defined as [22]

$$W = \begin{pmatrix} p(d_{0,0}) - p(d_{1,0}) & p(d_{2,0}) - p(d_{3,0}) \\ p(d_{0,1}) - p(d_{1,1}) & p(d_{2,1}) - p(d_{3,1}) \end{pmatrix} \quad (1)$$

where $p(d_{i,j})$ is the probability of the outcome $d_{i,j}$, defined as the detector d firing for the given settings α_i, β_j. For a causally structured two dimensional HV theory one should find that $\det(W) = 0$, whereas according to quantum mechanics for an ideal system $|\det(W)| = 1$. Figure 4(a) shows a comparison of the theoretical predictions and the experimental measurements, where the experimental data were obtained with and without the fair-sampling assumption (FSA). Under the FSA, we discard inconclusive results and postselect only coincidence events. The two-dimensional witness is calculated as $|\det(W)| = 0.778 \pm 0.005$ with the FSA, where the error is estimated from statistical error. Experimental errors mainly come from higher-order events in the SPDC and the control accuracy of EOM. Without the FSA, the two-dimensional witness is measured to be $|\det(W)| = 0.0268 \pm 0.0006$. The smaller magnitude of the dimensional witness is mainly due to the low collection efficiency ($\sim$ 20%). However, even without the FSA, the witness of the two dimensional HV, $|\det(W)| = 0$, is still violated by 44 standard deviations. This means that we have — with a great degree of confidence — shown that our experiment is inconsistent with a causally structured HV theory with two dimensions. Thus, this scheme is highly resilient to detection inefficiencies.

We also test compatibility with HV models that are dependent upon prior correlations that could influence the output of the interferometer. While our experiment rules out the causal influence of the operations that Alice and Bob perform on each other, it is possible that such correlations could be prepared long before the start of the experiment, and would not be forbidden by causality. We use the dimension witness [23, 26]

$$I_{\rm DW} = \langle D_{00}\rangle + \langle D_{01}\rangle + \langle D_{10}\rangle - \langle D_{11}\rangle - \langle D_{20}\rangle, \quad (2)$$

where $\langle D_{ij}\rangle = p(e_{i,j}) - p(d_{i,j})$, $p(e_{i,j})$ is the probability of the outcome e_{ij}, defined as the detector e firing for the given settings α_i, β_j (see Fig. 1(d)). The measurement settings are $\alpha_i \in \{\pi/4, 3\pi/4, -\pi/2\}$ and $\beta_j \in \{\pi/2, 0\}$ as be-

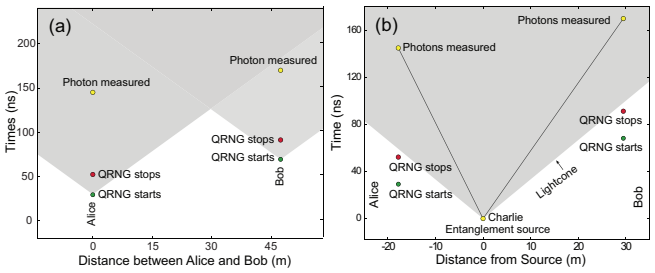

FIG. 3. Minkowski diagrams for the spacetime events related to Alice, Bob, and the source Charlie. All light cones are shaded gray. (a) Alice and Bob are space-like separated as the measurement is finished by Alice and Bob before information about the other party's measurement setting could have arrived. (b) The QRNGs at Alice and Bob finish picking a setting outside the light cone of the generation of an entangled photon pair by Charlie. All the events in our experiment are space-like separated.

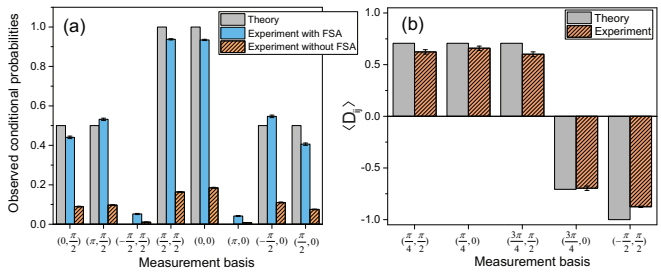

FIG. 4. (a) Conditional probability $p(d_{i,j})$ that detector d fires for given settings (α_i,β_j) chosen by Alice and Bob. Under the fair-sampling assumption (FSA) only coincidence events are post-selected. All the data were obtained in 1 minute continuous measurement. (b) Experimental results of the dimensional witness I_{DW}. The $\langle D_{ij}\rangle$ for the theoretical predictions and experimental measurement are shown as grey and hatched bars, respectively. All the data was obtained in a 1 minute continuous measurement. Error bars represent one standard deviation, deduced from propagated Poissonian counting statistics of the raw detection events.

fore. Any two-dimensional HV theory gives a strict bound of $I_{\rm DW}^{\rm HV} \leq 3$ even if Alice and Bob share pre-established correlations, while the quantum bound is $I_{\rm DW}^{\rm Q} = 1 + 2\sqrt{2} \approx 3.828$ [21, 27]. The data for this witness is shown in Fig. 4(b), and yields $I_{\rm DW}^{\rm Q} = 3.445 \pm 0.043$, with the FSA. The bound in this case is violated by 10 standard deviations.

The above shows that a causally structured two-dimensional HV model would be inconsistent with our experimental results. In addition to higher dimensional HV models, if one allows for the possibility of retrocausality (i.e. signaling backwards in time), it becomes possible to construct a HV theory that can account for statistics consistent with quantum experiment. Recall if full retrocausality is allowed, then a local HV model cannot be distinguished from quantum theory [28]. Interestingly, in Ref. [21] it is shown that quantum mechanics can be give bounds on types of retrocausal HV models that are allowed, by quantifying the degree of retrocausality contained in them. A measure of retrocausality $R_{B\to\Lambda}$ from Bob's measurement setting to the hypothetical hidden variable is bounded by

$$R_{B\to\Lambda} \geq R_{B\to\Lambda}^{\min} \equiv \max\left[\frac{I_{DW}-3}{4}, 0\right], \qquad (3)$$

where I_{DW} is the same dimensional witness used above. Here, $R_{B\to\Lambda} \in [0,1]$ is a value to quantify the strength of the causal influence of Bob's choice to the Alice's prepared state. The greater the value of $R_{B\to\Lambda}$ is, the stronger the retrocausal influence is, where $R_{B\to\Lambda} = 0$ is non-retrocausal, and $R_{B\to\Lambda} = 1$ is the strongest retrocausal classical models that Bob's choice can deterministically determine the prepared state. Using our experimental estimate we obtain $R_{B\to\Lambda}^{\min} = 0.114 \pm 0003$, in comparison to the ideal case where $R_{B\to\Lambda}^{\min} = (\sqrt{2}-1)/2 \approx 0.207$. The meaning of this is that, any retrocausal model with $R_{B\to\Lambda} < 0.114$ would not be able to reproduce our experimental results.

In summary, we have demonstrated a delayed-choice experiment by measuring a device-independent witness, and found that our experiment is inconsistent with the causally structured two-dimensional HV model. A key component in our experiment is to achieve space-like separation, which ensures that there is no communication occur between the devices and guarantees the devices of preparer and measurer are independent. Thus, our experiment preserves the same causal structure as the model provided in Ref. [21], and genuinely realizes the condition of independent devices required for the dimension witness in Ref. [22]. We have also excluded HV theories which assume correlation between Alice and Bob has been constructed in advance of the experiment, and we put a bound on the amount of retrocausality needed to explain our data without quantum mechanics. Our experiment shows that causal models can be used as a basis for testing of quantum mechanics, in a similar way to Bell and Leggett-Garg tests displaying effects that cannot be explained using a classical hidden variable theory.

ACKNOWLEDGMENTS

This work was supported by the National Natural Science Foundation of China, the Chinese Academy of Sciences, and the National Fundamental Research Program. J. P. D was supported by the National Science Foundation of the United States. T. B. is supported by the NSFC grant (D1210036A).

H.-L. Huang and Y.-H. Luo contributed equally to this work. During the final stages of manuscript preparation, we became aware of a similar work by Polino *et al.* [29], which was carried out simultaneously and independently.

Appendix A: Quantum random number generator module

The quantum random number generator (QRNG) module used in our experiment is based on random phase fluctuations of a spontaneous emission laser, which can be described math-

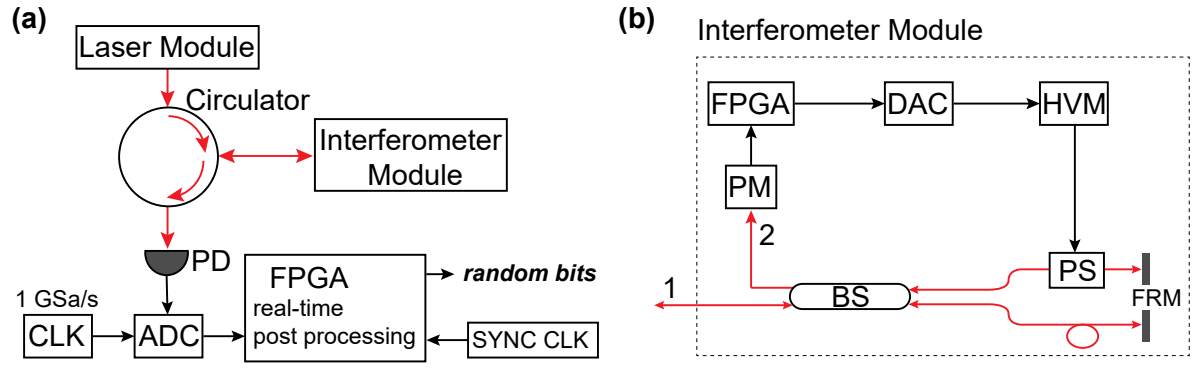

FIG. 5. (a) Scheme of the QRNG module, including laser module, three-port optical circulator, interferometer module, readout and postprocessing system. (b) Detail of interferometer module. The beam from laser module enters the interferometer via port 1. Then output port 2 is monitored by the feedback system, maintaining the optical path difference between two arms of the interferometer. The beam output from port 1 is directed to the sampling and post-processing system. PD: photondetector, CLK: clock, ADC: analog-to-digital converter, FPGA: field-programmable gate array, PM: powermeter, BS: beam splitter, DAC: digital-to-analog converter, HVM: high voltage module, PS: phase shifter, FRM: Faraday rotator mirror.

ematically as

$$E(t) = E_0 e^{i(\omega_0 t + \theta(t))}, \tag{A1}$$

where $\theta(t)$ is a gaussian distributed variable with quantum randomness [30]. By detecting the phase, together with digital post-processing, true random bits can be generated.

The scheme of the QRNG module is shown in Fig. 5(a). A laser, together with a thermoelectric cooler, constitutes the laser module. A 1550 nm laser is driven by a constant current slightly over threshold, making it work in spontaneous emission mode. The temperature of the laser is stabilized by a thermoelectric cooler. The beam emitted from the laser module is directed to the interferometer module via a three port optical circulator. Detail of the interferometer module is depicted in Fig. 5(b). It is an unbalanced Michelson interferometer with optical path difference $\omega_0 \Delta T$, which is set to $2m\pi + \pi/2$. Two Faraday rotator mirrors (FRMs) can effectively remove the influence of polarization. In this way, the intensity at the output port 1 is $I(t) = 2E_0^2\big(1+\sin\Delta\theta(t)\big)$, which is then detected by a high speed InGaAs photodetector. After filtering the DC signal, the quantum signal acquired by photodetector, satisfying $I(t) \propto P\sin(\Delta\theta(t)) \approx P\Delta\theta(t)$, is digitized to an 8-bit digital signal per sample by ADC (AT84AD001B) with a clock rate of 1 GSa/s. Then, the raw data is fed into a FPGA. Real-time post-processing based on Toeplitz hashing matrix [30] is implemented, which has an overhead of less than 25 ns and improves the quality of the random bits. To synchronize all the devices used in the experiment, a synchronization clock (500 kHz) is used. For the QRNG module, one random bit is output once a synchronization clock pulse is detected. The random bit is then transmitted to the modulator drivers, driving an electro-optic modulator (EOM).

As is stated above, the stability of $\omega_0 \Delta T$ is crucial. To stabilize $\omega_0 \Delta T$, as is shown in Fig. 5(b), port 2 is monitored by a power meter (PM), a PID controller based on a FPGA is used to send feedback data to a DAC, which controls a high voltage module (HVM). A HVM drives the phase shifter (PS), maintaining optical path difference between two arms of the interferometer at a high level. In such a process, the influence of phase fluctuations θ is wiped out by time averaging, due to the fact that $\Delta\langle\theta(t)\rangle = 0$.

For more details about the QRNG, we refer the reader to Refs. [31–33].

Appendix B: The performance of the photon source

In our experiment, the repetition rate of the whole system is 500kHz. The polarization entangled quantum state $|H\rangle_A|H\rangle_B + |V\rangle_A|V\rangle_B$ is generated via spontaneous parametric down-conversion (SPDC) using a sandwich-like $\beta-BaB_2O_4$ (BBO) bulk crystal and a half-wave plate (HWP). The probability p of generating a single photon pair per pump pulse is $p \approx 0.018$, which means that the pair production rate is ∼9kHz, and probability of the undesired noise contribution from double-pair emission is $p^2 \approx (0.018)^2$. The overall efficiency of our entangled photon source is ∼20% (with 3nm and 8nm filtering for the e and o photon, respectively) due to fiber loss, fiber flange loss, coupling efficiency, the transmittance of the EOM, and detector efficiency (∼60%). Thus, the brightness (or detection rate) of entangled photon-pair source is ∼0.36kHz.

We further quantified the single-photon purity of the heralded single-photon source with the second-order correlation function at zero time delay $g^2(0)$. The smaller $g^2(0)$ is, the higher the purity of the heralded single-photon source is. We performed the experiments with various levels of pair production rate to demonstrate the trade-off between the heralded single-photon purity and the pair production rate of the SPDC sources (see Fig. 6). The $g^2(0)$ of the heralded single-photon source in our experiment is $g^2(0) = 0.0367 \pm 0.0005$ for a pair production rate of ∼9kHz.

In addition, we measured one photon of the entangled state in the basis $\{|H\rangle_A \pm |V\rangle_A\}$, postselected it in the state

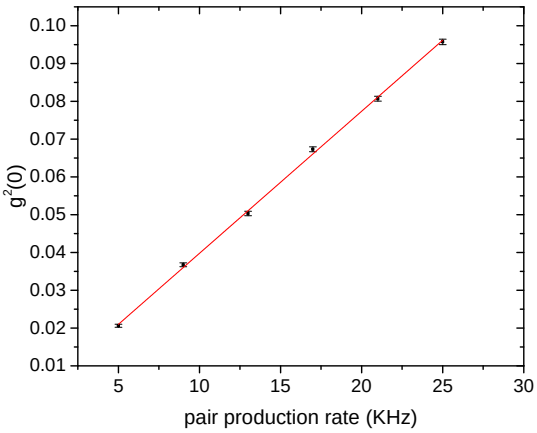

FIG. 6. Experimentally measured relationship between the second-order correlation function at zero delay $g^2(0)$ and pair production rate. The $g^2(0)$ data shown seems to have a linear relationship with the pair production rate, and is therefore linearly fitted. The higher the pair production rate is, the larger the value of $g^2(0)$ becomes.

$|H\rangle_A + |V\rangle_A$, and then measured the other photon in the basis $\{|H\rangle_B \pm e^{i\beta_j}|V\rangle_B\}$, where the phase β_j is changed as $0 \to \pi \to 2\pi$. Figure 7 shows the measurement results, the data are fitted to sinusoidal fringes and consistent with the theoretical prediction $(1+\cos\beta_j)/2$. The fidelity of the entangled state is ∼96%.

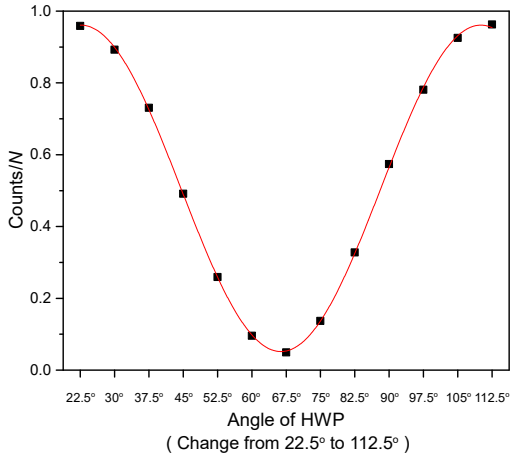

FIG. 7. Experimental measurement of the entangled state $|H\rangle_A|H\rangle_B + |V\rangle_A|V\rangle_B$. We fixed one photon of the EPR state at $|H\rangle_A + |V\rangle_A$, and then measured another photon in the basis $|H\rangle_B + e^{i\beta_j}|V\rangle_B$. The phase β_j is changed as $0 \to \pi \to 2\pi$ by changing the angle of HWP from 22.5° to 112.5°.

[1] N. Bohr, in *Niels Bohr Collected Works*, Vol. 7 (Elsevier, 1996) pp. 339–381.
[2] A. Einstein, B. Podolsky, and N. Rosen, Phys. Rev. **47**, 777 (1935).
[3] J. v. Neumann, *Mathematische Grundlagen der Quantenmechanik*, Vol. 932 (Springer, 1932).
[4] J. Bell *et al.*, Physics Physique Fizika **1**, 195 (1964).
[5] J. A. Wheeler, in *Mathematical foundations of quantum theory* (Elsevier, 1978) pp. 9–48.
[6] J. A. Wheeler, W. H. Zurek, and L. E. Ballentine, Am. J. Phys. **52**, 955 (1984).
[7] T. Hellmuth, H. Walther, A. Zajonc, and W. Schleich, Phys. Rev. A **35**, 2532 (1987).
[8] B. Lawson-Daku, R. Asimov, O. Gorceix, C. Miniatura, J. Robert, and J. Baudon, Phys. Rev. A **54**, 5042 (1996).
[9] Y.-H. Kim, R. Yu, S. P. Kulik, Y. Shih, and M. O. Scully, Phys. Rev. Lett. **84**, 1 (2000).
[10] A. Zeilinger, G. Weihs, T. Jennewein, and M. Aspelmeyer, Nature **433**, 230 (2005).
[11] V. Jacques, E. Wu, F. Grosshans, F. Treussart, P. Grangier, A. Aspect, and J.-F. Roch, Science **315**, 966 (2007).
[12] F. Vedovato, C. Agnesi, M. Schiavon, D. Dequal, L. Calderaro, M. Tomasin, D. G. Marangon, A. Stanco, V. Luceri, G. Bianco, G. Vallone, and P. Villoresi, Sci. Adv. **3**, e1701180 (2017).
[13] R. Ionicioiu and D. R. Terno, Phys. Rev. Lett. **107**, 230406 (2011).
[14] R. Ionicioiu, T. Jennewein, R. B. Mann, and D. R. Terno, Nat. Commun. **5**, 3997 (2014).
[15] F. Kaiser, T. Coudreau, P. Milman, D. B. Ostrowsky, and S. Tanzilli, Science **338**, 637 (2012).
[16] A. Peruzzo, P. Shadbolt, N. Brunner, S. Popescu, and J. L. O'Brien, Science **338**, 634 (2012).
[17] A. S. Rab, E. Polino, Z.-X. Man, N. B. An, Y.-J. Xia, N. Spagnolo, R. L. Franco, and F. Sciarrino, Nat. Commun. **8**, 915 (2017).
[18] K. Liu, Y. Xu, W. Wang, S.-B. Zheng, T. Roy, S. Kundu, M. Chand, A. Ranadive, R. Vijay, Y. Song, L. Duan, and L. Sun, Sci. Adv. **3**, e1603159 (2017).
[19] J. Pearl, *Causality* (Cambridge university press, 2009).
[20] M. Ringbauer, C. Giarmatzi, R. Chaves, F. Costa, A. G. White, and A. Fedrizzi, Sci. Adv. **2**, e1600162 (2016).
[21] R. Chaves, G. B. Lemos, and J. Pienaar, Phys. Rev. Lett. **120**, 190401 (2018).
[22] J. Bowles, M. T. Quintino, and N. Brunner, Phys. Rev. Lett. **112**, 140407 (2014).
[23] R. Gallego, N. Brunner, C. Hadley, and A. Acín, Phys. Rev. Lett. **105**, 230501 (2010).
[24] A. J. Leggett and A. Garg, Phys. Rev. Lett. **54**, 857 (1985).
[25] X.-L. Wang, L.-K. Chen, W. Li, H.-L. Huang, C. Liu, C. Chen, Y.-H. Luo, Z.-E. Su, D. Wu, Z.-D. Li, *et al.*, Phys. Rev. Lett. **117**, 210502 (2016).
[26] J. Ahrens, P. Badziag, A. Cabello, and M. Bourennane, Nat. Phys. **8**, 592 (2012).
[27] A. Tavakoli, J. Kaniewski, T. Vértesi, D. Rosset, and N. Brunner, Phys. Rev. A **98**, 062307 (2018).
[28] D. Lazarovici, Proc. R. Soc. A **471**, 20140454 (2015).
[29] E. Polino, I. Agresti, D. Poderini, G. Carvacho, G. Milani, G. B. Lemos, R. Chaves, and F. Sciarrino, arXiv:1806.00211 (2018).

[30] X. Ma, F. Xu, H. Xu, X. Tan, B. Qi, and H.-K. Lo, Phys. Rev. A **87**, 062327 (2013).
[31] Y.-Q. Nie, H.-F. Zhang, Z. Zhang, J. Wang, X. Ma, J. Zhang, and J.-W. Pan, Appl. Phys. Lett. **104**, 051110 (2014).
[32] Y.-Q. Nie, L. Huang, Y. Liu, F. Payne, J. Zhang, and J.-W. Pan, Rev. Sci. Instrum. **86**, 063105 (2015).
[33] X.-G. Zhang, Y.-Q. Nie, H. Zhou, H. Liang, X. Ma, J. Zhang, and J.-W. Pan, Rev. Sci. Instrum. **87**, 076102 (2016).